Supporting Information for

Magnetic-ferroelectric synergic control of multilevel conducting states in van der Waals multiferroic tunnel junction towards in-memory computing

Zhou Cui[1], Baisheng Sa[1,*], Kan-Hao Xue[2], Yinggan Zhang[3], Rui Xiong[1], Cuilian Wen[1], Xiangshui Miao[2] and Zhimei Sun[4,*]

[1]*Multiscale Multiscale Computational Materials Facility & Materials Genome Institute, School of Materials Science and Engineering, Fuzhou University, Fuzhou 350108, China.*

[2]*School of Integrated Circuits, Huazhong University of Science and Technology, Wuhan 430074, China*

[3]*College of Materials, Fujian Provincial Key Laboratory of Theoretical and Computational Chemistry, Xiamen University, Xiamen 361005, P. R. China*

[4]*School of Materials Science and Engineering, and Center for Integrated Computational Materials Science, International Research Institute for Multidisciplinary Science, Beihang University, Beijing 100191, P. R. China*

Corresponding Author: bssa@fzu.edu.cn (B. Sa); zmsun@buaa.edu.cn (Z. Sun)

Table S1 The formation energy E_{form} (meV) of various stacking configurations for In_2S_3/Mn_2Se_3 and $Mn_2Se_3/TiTe_2$ heterostructures.

Stacking	Mn_2Se_3/In_2S_3-P↑	Mn_2Se_3/In_2S_3-P↓	$Mn_2Se_3/TiTe_2$
I	-174.45	-159.05	-366.10
II	-91.86	-122.61	-260.24
III	-171.52	-157.30	-335.75
IV	-170.45	-157.90	-262.01
V	-174.44	-159.87	-362.18
VI	-92.32	-82.23	-336.22

Table S2 The calculated SIE and RA ($\Omega \cdot \mu m^2$) for FE-R-1IS and FE-L-1IS MFTJs.

MFTJ	PC state		APC state	
	SIE	RA	SIE	RA
FE-R-1IS	98.27 %	0.14	9.65 %	0.79
FE-L-1IS	98.05 %	0.13	33.23 %	0.61

Table S3 The formation energy E_{form} (meV) of various stacking configurations for bilayer In_2S_3 in AFE-T, AFE-H and FE states.

Stacking	AFE-T	AFE-H	FE
I	-235.52	-218.60	-229.12
II	-146.01	-140.73	-145.42
III	-232.17	-220.01	-229.01
IV	-234.48	-219.83	-229.81
V	-234.48	-219.83	-228.87
VI	-145.41	-140.39	-145.05

Table S4 The calculated SIE and RA ($\Omega\cdot\mu m^2$) for AFE-T-2IS, AFE-H-2IS, FE-R-2IS and FE-L-2IS MFTJs.

MFTJ	PC state		APC state	
	SIE	RA	SIE	RA
AFE-T-2IS	99.8%	0.14	2.1%	8.02
AFE-H-2IS	99.0%	0.56	10.5%	8.76
FE-R-2IS	97.3%	2.61	18.4%	10.75
FE-L-2IS	97.3%	2.59	27.1%	11.30

Table S5 The spin-dependent conductances (e^2/h), TMR and TER ratios of the MFTJ with AFE-T-2IS, AFE-H-2IS, FE-R-2IS and FE-L-2IS states under the bias of 40 meV.

MFTJ	PC state			APC state			TMR
	Spin up	Spin down	Total-PC	Spin up	Spin down	Total-APC	
AFE-T-2IS	2.32×10^{-2}	2.07×10^{-5}	2.32×10^{-2}	2.45×10^{-4}	1.82×10^{-4}	4.28×10^{-4}	5329 %
AFE-H-2IS	5.79×10^{-3}	2.61×10^{-5}	5.81×10^{-3}	1.55×10^{-4}	1.51×10^{-4}	3.06×10^{-4}	1799 %
FE-R-2IS	1.74×10^{-3}	1.46×10^{-5}	1.76×10^{-3}	1.35×10^{-4}	1.00×10^{-4}	2.35×10^{-4}	646 %
FE-L-2IS	1.56×10^{-3}	1.64×10^{-5}	1.57×10^{-3}	1.30×10^{-4}	1.40×10^{-4}	2.70×10^{-4}	484 %
$TER_{AFE\text{-}T/FE\text{-}L}$			1376 %			59 %	
$TER_{AFE\text{-}H/FE\text{-}L}$			269 %			13 %	
$TER_{FE\text{-}R/FE\text{-}L}$			12 %			13 %	

Table S6 The spin-dependent conductances (e^2/h), TMR and TER ratios of the MFTJ with AFE-T-2IS, AFE-H-2IS, FE-R-2IS and FE-L-2IS states under the bias of 60 meV.

MFTJ	PC state			APC state			TMR
	Spin up	Spin down	Total-PC	Spin up	Spin down	Total-APC	
AFE-T-2IS	2.09×10^{-2}	2.29×10^{-5}	2.10×10^{-2}	2.53×10^{-4}	1.93×10^{-4}	4.46×10^{-4}	4600 %
AFE-H-2IS	5.11×10^{-3}	2.79×10^{-5}	5.14×10^{-3}	1.85×10^{-4}	1.64×10^{-4}	3.49×10^{-4}	1374 %
FE-R-2IS	1.47×10^{-3}	1.54×10^{-5}	1.49×10^{-3}	1.45×10^{-4}	8.87×10^{-5}	2.34×10^{-4}	535%
FE-L-2IS	1.32×10^{-3}	1.76×10^{-5}	1.34×10^{-3}	1.26×10^{-4}	1.43×10^{-4}	2.69×10^{-4}	396 %
$TER_{AFE-T/FE-L}$			1470 %			66 %	
$TER_{AFE-H/FE-L}$			285 %			29 %	
$TER_{FE-R/FE-L}$			11 %			13 %	

Table S7 The spin-dependent conductances (e^2/h), TMR and TER ratios of the MFTJ with AFE-T-2IS, AFE-H-2IS, FE-R-2IS and FE-L-2IS states under the bias of 80 meV.

MFTJ	PC state			APC state			TMR
	Spin up	Spin down	Total-PC	Spin up	Spin down	Total-APC	
AFE-T-2IS	1.76×10^{-2}	2.15×10^{-5}	1.77×10^{-2}	2.45×10^{-4}	1.70×10^{-4}	4.15×10^{-4}	4154 %
AFE-H-2IS	4.42×10^{-3}	2.77×10^{-5}	4.44×10^{-3}	1.76×10^{-4}	1.60×10^{-4}	3.36×10^{-4}	1222 %
FE-R-2IS	1.48×10^{-3}	1.52×10^{-5}	1.50×10^{-3}	1.61×10^{-4}	7.99×10^{-5}	2.41×10^{-4}	521 %
FE-L-2IS	1.33×10^{-3}	1.79×10^{-5}	1.35×10^{-3}	1.34×10^{-4}	1.43×10^{-4}	2.76×10^{-4}	389 %
$TER_{AFE-T/FE-L}$			1207 %			50 %	
$TER_{AFE-H/FE-L}$			229 %			22 %	
$TER_{FE-R/FE-L}$			11 %			13 %	

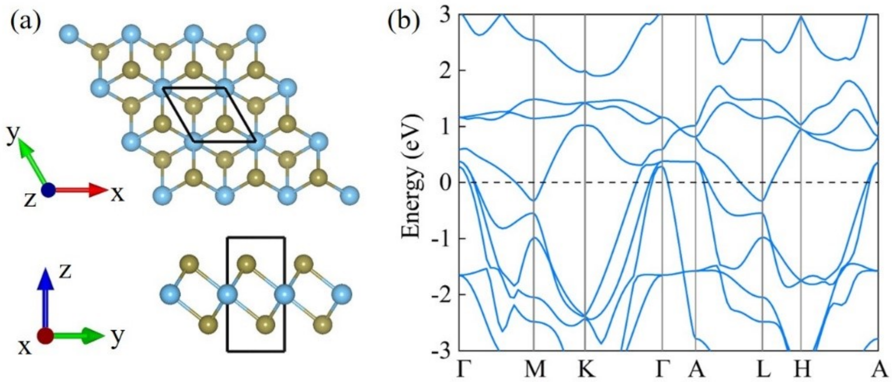

Fig. S1 The crystal structure and band structures of bulk TiT_2.

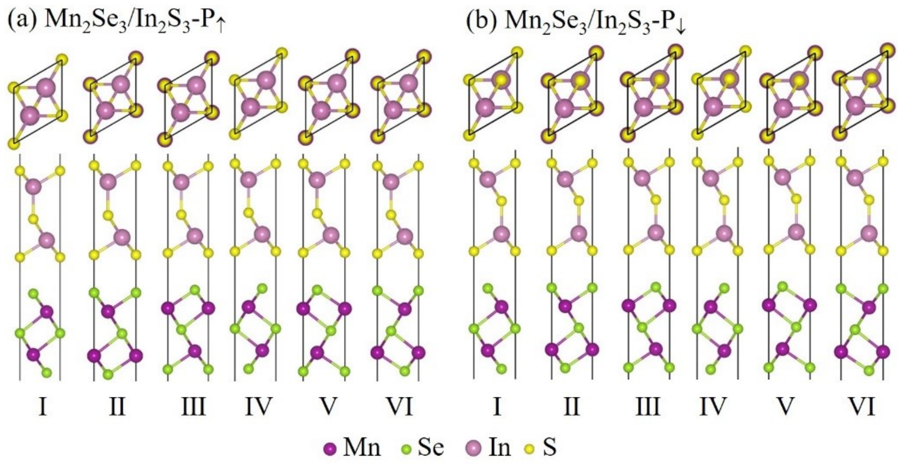

Fig. S2 The different stacking configurations of (a) In_2S_3/Mn_2Se_3-P↑ and (b) Mn_2Se_3/In_2S_3-P↓ heterostructures.

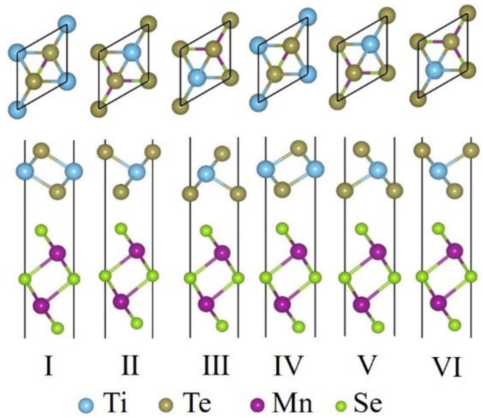

Fig. S3 The different stacking configurations of $Mn_2Se_3/TiTe_2$ heterostructures.

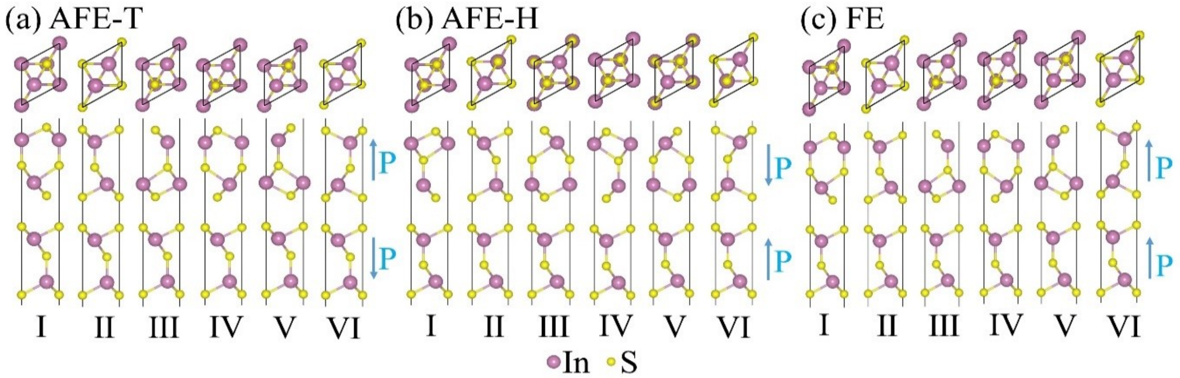

Fig. S4 The different stacking configurations of bilayer In_2S_3 with ferroelectric polarizations in (a) AFE-T, (b) AFE-H and (c) FE states.

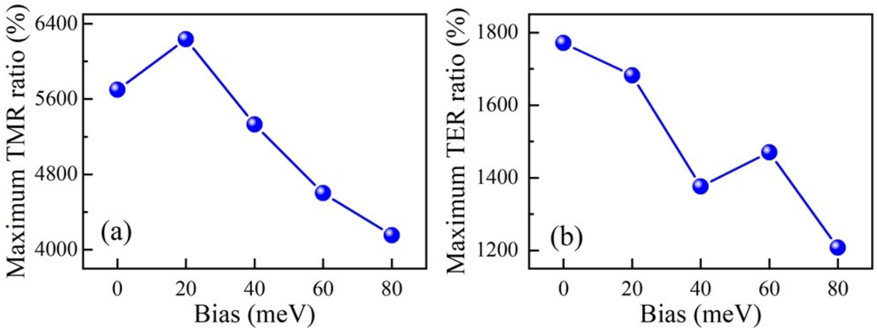

Fig. S5 The maximum (a) TMR and (b) TER ratios of the MFTJ with bilayer In_2S_3 as the tunnel barrier under different finite biases.

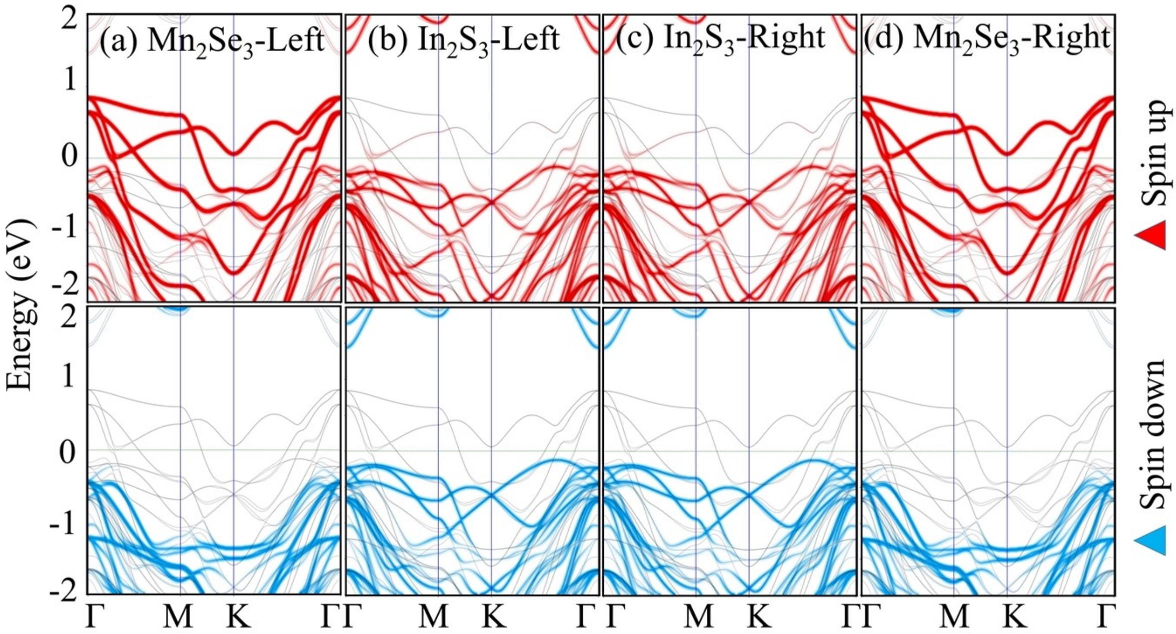

Fig. S6 The spin-dependent projected band structures of (a) Mn_2Se_3-Left, (b) In_2S_3-Left, (c) In_2S_3-Right and (d) Mn_2Se_3-Right layers in AFE-T-2IS MFTJ.

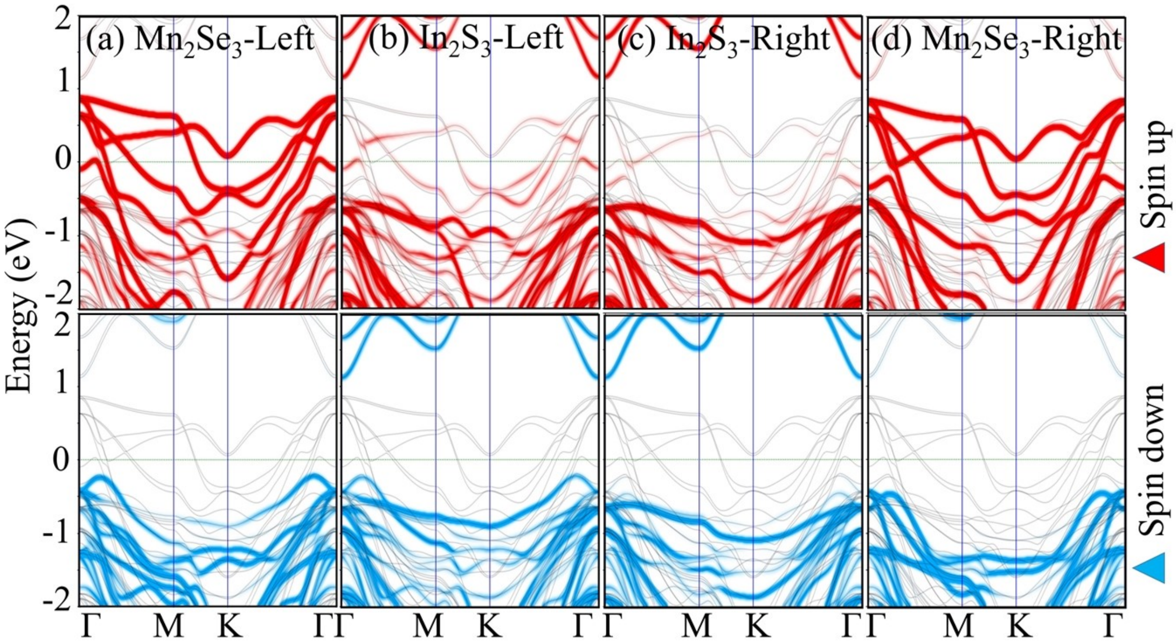

Fig. S7 The spin-dependent projected band structures of (a) Mn_2Se_3-Left, (b) In_2S_3-Left, (c) In_2S_3-Right and (d) Mn_2Se_3-Right layers in AFE-H-2IS MFTJ.

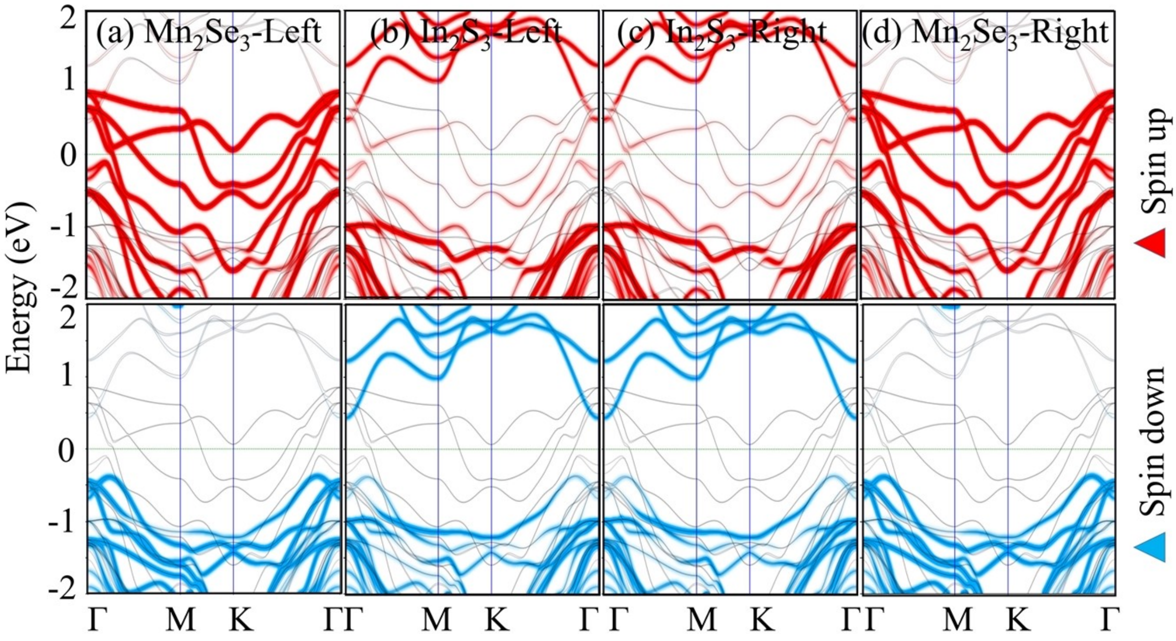

Fig. S8 The spin-dependent projected band structures of (a) Mn_2Se_3-Left, (b) In_2S_3-Left, (c) In_2S_3-Right and (d) Mn_2Se_3-Right layers in FE-R-2IS MFTJ.

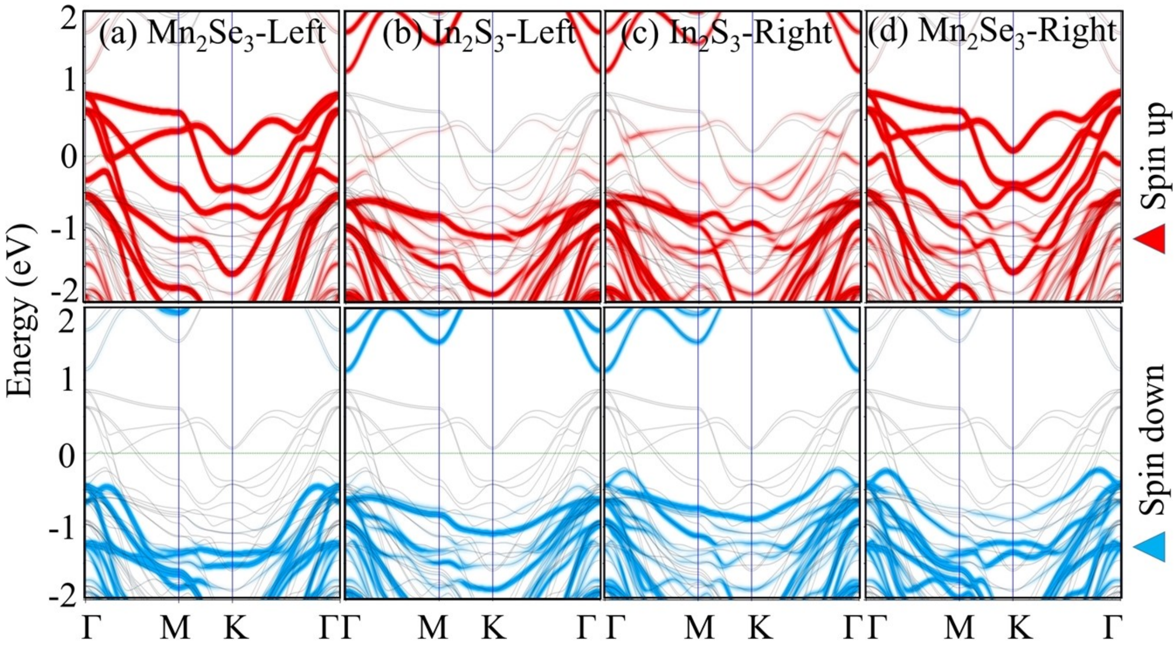

Fig. S9 The spin-dependent projected band structures of (a) Mn_2Se_3-Left, (b) In_2S_3-Left, (c) In_2S_3-Right and (d) Mn_2Se_3-Right layers in FE-L-2IS MFTJ.